C. R. Mecanique 338 (2010) 402–411

Contents lists available at ScienceDirect

Comptes Rendus Mecanique

www.sciencedirect.com

Inverse problems

An adaptive procedure for defect identification problems in elasticity

Une procédure adaptative pour l'identification de défauts en élasticité

Sergio Gutiérrez *, J. Mura

Department of Structural and Geotechnical Engineering, Pontificia Universidad Católica de Chile, casilla 306 Correo 22, Santiago, Chile

ARTICLE INFO

Article history:
Available online 16 August 2010

Keywords:
Continuum mechanics
Inverse problems
Defects in solids
Homogenization

Mots-clés :
Milieux continus
Problèmes inverses
Défauts dans les solides
Homogénéisation

ABSTRACT

In the context of inverse problems in mechanics, it is well known that the most typical situation is that neither the interior nor all the boundary is available to obtain data to detect the presence of inclusions or defects. We propose here an adaptive method that uses loads and measures of displacements only on part of the surface of the body, to detect defects in the interior of an elastic body. The method is based on Small Amplitude Homogenization, that is, we work under the assumption that the contrast on the values of the Lamé elastic coefficients between the defect and the matrix is not very large. The idea is that given the data for one loading state and one location of the displacement sensors, we use an optimization method to obtain a guess for the location of the inclusion and then, using this guess, we adapt the position of the sensors and the loading zone, hoping to refine the current guess.

Numerical results show that the method is quite efficient in some cases, using in those cases no more than three loading positions and three different positions of the sensors.

RÉSUMÉ

Dans le contexte de problèmes inverses en mécanique, il est bien connu que la situation typique est celle où ni l'intérieur du solide ni la totalité de sa frontière ne sont disponibles pour recueillir des données permettant l'identification d'inclusions ou de défauts. Nous proposons ici une approche adaptative qui utilise la connaissance du chargement et de déplacements mesurés sur une portion de la frontière pour détecter des défauts intérieurs à un solide élastique. Cette méthode repose sur l'homogénéisation à faible amplitude, c'est-à-dire l'hypothèse que le contraste des coefficients de Lamé entre les défauts et la matrice est modéré. A l'aide des données correspondant à un chargement et une configuration de capteurs, une méthode d'optimisation permet d'estimer l'emplacement de l'inclusion, cette estimation étant ensuite utilisée pour adapter le choix du chargement et de l'emplacement des capteurs et raffiner la solution. Des exemples numériques, reposant sur au maximum trois configurations successives de chargement et de capteurs, montrent l'efficacité de la méthode dans certains cas.

* Corresponding author.
E-mail addresses: sgutierr@ing.puc.cl (S. Gutiérrez), jamura@ing.puc.cl (J. Mura).

1631-0721/$ – see front matter
doi:10.1016/j.crme.2010.07.004

1. Introduction

Tools devised originally for optimal design have been used to try to solve inverse problems by several authors [1–4] and many others. The idea is to look for the optimal distribution of material in order that the boundary measurements coincide, as much as possible, with the data being measured in the laboratory. Then the modelling uses a mixture of two phases with different elastic properties and their distributions inside the body will be the optimization variable.

However, one nontrivial difficulty is added to the problem, because, in general, it will be necessary to relax it, which can be done in different ways: using full homogenization, doing so-called partial relaxations, namely, allowing only for certain microstructures to be considered in the minimization. Yet another way is by quasi-convexification.

Here we follow the homogenization approach and benefit from the results obtained in the case of small oscillations in the elastic parameters. This is a situation where the asymptotic homogenization formulas become more explicit, as it was shown in the pioneer work of Luc Tartar [5]. Much later in [6] those formulas were put to use in terms of obtaining a rather general optimal design algorithm, the application of which to inverse problems was first presented in [4], but only in the context of diffusion problems and without any study of stability issues, like noisy measurements or erroneous characterization of the inclusion one is looking for. These issues were addressed in the context of elasticity in [7] and the numerical results are quite encouraging. Namely the method is quite stable under noisy displacement measures and erroneous values of either the contrast parameter or the volume of the inclusion. Moreover, the method is very robust in the sense that in most cases it gives the same final location of the inclusion, independently of the initial configuration given to the optimization algorithm.

The method, however, seems to have two main drawbacks: first it deals efficiently only with situations where the amplitude is relatively small, up to fifty percent sometimes, but more often no more than thirty percent contrast can be permitted; the other, more important, drawback is that the inclusion should be close to the surface. This seeming restriction on the applicability of the method, gave us the idea to find an adaptive way to select the locations of the load and the sensors to pinpoint the inclusion using several experiments. This is the purpose of this work.

The content of the article is as follows. Section 2 presents the definition of the problem and its formulation in an optimization framework. Section 3 proposes the adaptive procedure to improve the quality of the results. Then in Section 4 we present and discuss two examples where adaptivity plays an important role. Finally, in Section 5 some closing remarks and general conclusions are provided.

2. Statement of the problem

We consider a solid body denoted by $\Omega \subset \mathbb{R}^N$ $(N = 2, 3)$ with an embedded defect. The position of the defect, associated with phase 1, is marked by the characteristic function χ^r of a certain region, later this region will be referred to as the "real" location of the defect. The rest of the body is filled with the matrix (phase 0). For both phases, we associate symmetric positive-definite elasticity tensors C_0 and C_1, which enable us to describe the tensor for the whole body as:

$$C^r(x) = \big(1 - \chi^r(x)\big)C_0 + \chi^r(x)C_1 \quad \forall x \in \Omega$$

We assume the boundary of Ω, that is denoted by $\partial\Omega$, to be piecewise sufficiently smooth and divided in two disjoint parts $\partial\Omega = \Gamma_D \cup \Gamma_N$, where Dirichlet and Neumann boundary conditions are imposed, respectively. Let $V = \{\varphi \in [H^1(\Omega)]^N$ s.t. $v = 0$ on $\Gamma_D\}$ and $u^r \in V$ solution to the boundary value problem of elasticity, which in variational form is

$$\int_\Omega C^r \varepsilon\big(u^r\big) : \varepsilon(\varphi)\,\mathrm{d}x = \int_\Omega f \cdot \varphi\,\mathrm{d}x + \int_{\Gamma_N} g \cdot \varphi\,\mathrm{d}s \quad \forall \varphi \in V \tag{1}$$

where $\varepsilon(u^r)$ is the infinitesimal strain tensor for the small displacement u^r and f, g are known external loads satisfying the usual regularity requirements to have existence and uniqueness for the displacement field u^r.

Let us then suppose that we have a measurement of u^r on $\Gamma \subset \Gamma_N$. This information, added to the knowledge of g and f, will help in the detection of the defect.

Then, in order to detect the inclusion, our approach consists of constructing a sequence of guesses $\{\chi^{(k)}\}_{k\geqslant 1}$ for the defect location, associated to the solution of

$$\int_\Omega C^{(k)} \varepsilon\big(u^{(k)}\big) : \varepsilon(\varphi)\,\mathrm{d}x = \int_\Omega f \cdot \varphi\,\mathrm{d}x + \int_{\Gamma_N} g \cdot \varphi\,\mathrm{d}s \quad \forall \varphi \in V \tag{2}$$

where $C^{(k)}(x) = (1 - \chi^{(k)}(x))C_0 + \chi^{(k)}(x)C_1$ for any $x \in \Omega$, such that the sequence $\{\chi^{(k)}\}_{k\geqslant 1}$ minimizes the objective function

$$J\big(\chi^{(k)}\big) = \int_\Gamma \big\|u^{(k)} - u^r\big\|^2\,\mathrm{d}s \tag{3}$$

in other words, we want to approximate the given experimental data u^r with the one obtained from the k-th guess and in this manner hopefully obtain that $\chi^{(k)}$ converges to χ^r.

We define a set of admissible designs (the feasible set) by assuming that the two phases have prescribed volumes: $\Theta|\Omega|$ for phase 1 and $(1-\Theta)|\Omega|$ for phase 0, with $\Theta \in (0,1)$,

$$\mathcal{U}_{ad} = \left\{ \chi \in L^\infty\big(\Omega; \{0,1\}\big) \text{ s.t.} \int_\Omega \chi(x)\,\mathrm{d}x = \Theta|\Omega| \right\}$$

Thus, our statement is to find the location of the defect from the optimization problem

$$\chi^* = \operatorname{argmin}\big\{ J(\chi):\ \chi \in \mathcal{U}_{ad} \big\} \tag{4}$$

However, it is well known that this problem is ill-posed, see, for example, [8,9] and references therein. The problem being that the limit of a sequence of characteristic functions might not be well defined as a characteristic function.

There are several alternatives to try to circumvent this difficulty. One is to restrict the possible limits of the sequence of characteristic functions, which in our context will probably limit the kind of inclusions we can detect. Another possibility is to relax the problem and consider all possible limits, this implies that we should know the set of all the elastic tensors we can generate by homogenizing a mixture of phases 0 and 1, which is not known. In the literature this is known as the G-closure problem. The solution to this problem is asymptotically known in the case when the contrast parameter η is arbitrarily small, since the work in [5], therefore we profit from that here and develop an algorithm to detect so-called weak defects through an adaptive set of loads and measures.

Even though the relaxation will introduce the additional complication of considering a microstructure, that we know does not exist in the geometry we are trying to recover, it provides a mathematical framework that ensures the existence of a solution to the minimization problem, which is not so in the context of problem (4), as it is well documented in the structural optimization literature.

Now we recall the asymptotic approximation, based on the small amplitude assumption, used to derive the optimal design algorithm in [6] and applied to inverse problems in [4] and [7]. This asymptotic approach will provide the existence of a minimizer and, additionally, the characterization of the corresponding limit of elasticity tensors, when the contrast between phases 0 and 1 is small enough. This is achieved by considering a two-phase microstructure and the relaxation of $\chi \in L^\infty(\Omega; \{0,1\})$ to a local density or proportion $\theta \in L^\infty(\Omega; [0,1])$ in the sense of the weak-$\star$ topology.

We denote by η the amplitude (contrast or aspect ratio) between the two materials associated to the elasticity tensors C_0 and C_1 such that the amplitude or contrast η is small, then we perform a second order expansion in the state equation and in the objective function. We can consider a quite general relationship between C_0 and C_1, namely that $C_1 = C_0 + \eta D$, with D a forth order symmetric tensor and η small enough in absolute value, so that C_1 is still positive definite. Hence, one could have two materials with different Poisson ratios, for example. However, this will render difficult to give a physical meaning to the value of the contrast parameter and the computation of the corrector term involving tensor M in formula (11) below, has to be redone for the specific tensor D in the way used in [8] to obtain m_0. Therefore we prefer to work in the particular case when $D = C_0$, moreover C_0 will be an isotropic elasticity tensor. Hence, we assume that $C_1 = (1+\eta)\,C_0$, this means that

$$C^r = \big(1 + \eta\chi^r\big)C_0 \quad \text{and} \quad C^{(k)} = \big(1 + \eta\chi^{(k)}\big)C_0$$

which, in the case when C_0 is isotropic implies that $\lambda_1 = (1+\eta)\lambda_0$ and $\mu_1 = (1+\eta)\mu_0$, where λ_i and μ_i $(i = 0, 1)$ are the Lamé parameters associated with tensors C^i, respectively. By relating these parameters with the Young modulus E and the Poisson ratio ν, one can obtain that $E_1 = (1+\eta)E_0$ and $\nu_1 = \nu_0$, thus the inclusion is stiffer than the matrix if $\eta > 0$ (otherwise more flexible), but both materials will have the same Poisson ratio. Since $E_1 > 0$, the range of η is restricted to $(-1, +\infty)$, but in the sequel we shall assume that η is small, i.e. $|\eta| \ll 1$.

Since the coefficient tensor $C^{(k)}$ is an affine function of η, the solution $u^{(k)} \in V$ is analytic with respect to η and we can write

$$u^{(k)} = u_0^{(k)} + \eta u_1^{(k)} + \eta^2 u_2^{(k)} + O\big(\eta^3\big) \tag{5}$$

plugging this ansatz in (2) for a given $\chi^{(k)}$ yields a cascade of three variational problems for $(u_0^{(k)}, u_1^{(k)}, u_2^{(k)})$:

$$\int_\Omega C_0\varepsilon\big(u_0^{(k)}\big) : \varepsilon(\varphi)\,\mathrm{d}x = \int_\Omega f\cdot\varphi\,\mathrm{d}x + \int_{\Gamma_N} g\cdot\varphi\,\mathrm{d}s \quad \forall\varphi \in V \tag{6}$$

$$\int_\Omega C_0\varepsilon\big(u_1^{(k)}\big) : \varepsilon(\varphi)\,\mathrm{d}x = -\int_\Omega \chi^{(k)} C_0\varepsilon\big(u_0^{(k)}\big) : \varepsilon(\varphi)\,\mathrm{d}x \quad \forall\varphi \in V \tag{7}$$

$$\int_\Omega C_0\varepsilon\big(u_2^{(k)}\big) : \varepsilon(\varphi)\,\mathrm{d}x = -\int_\Omega \chi^{(k)} C_0\varepsilon\big(u_1^{(k)}\big) : \varepsilon(\varphi)\,\mathrm{d}x \quad \forall\varphi \in V \tag{8}$$

We notice that $u_0^{(k)}$ does not depend on $\chi^{(k)}$, so we drop the superscript. Therefore we have a procedure to obtain $(u_0, u_1^{(k)}, u_2^{(k)})$ and now we turn to see the way they participate in the objective function. In a likewise manner, we get the truncated Taylor expansion of (3) up to second order in η, which depends only on u_0, u_1 and u_2

$$\mathcal{J}_{sa}(u_0, u_1, u_2) = \int_\Gamma \|u_0 - u^r\|^2 \,\mathrm{d}s + 2\eta \int_\Gamma (u_0 - u^r)\cdot u_1 \,\mathrm{d}s + \eta^2 \int_\Gamma \big(2(u_0 - u^r)\cdot u_2 + u_1 \cdot u_1\big)\,\mathrm{d}s \tag{9}$$

Therefore we propose to solve instead of (4) the following optimal design problem

$$\inf_{\chi\in\mathcal{U}_{ad}} \big\{ J_{sa}(\chi) = \mathcal{J}_{sa}(u_0, u_1, u_2)\big\} \tag{10}$$

To solve this problem we relax it, as it was done in [6]. To write the relaxation we need to consider the limiting problems for problems (7) and (8). First we notice that if $\chi^{(k)}$ belongs to a sequence that converges weakly to θ with $u_1^{(k)} \rightharpoonup u_1$ and $u_2^{(k)} \rightharpoonup u_2$. For the first order equation (7), due to the linear dependency on $\chi^{(k)}$ we know that at the limit, u_1 solves the same problem as $u_1^{(k)}$ when replacing $\chi^{(k)}$ by θ. However, this is not the case for the limit of $u_2^{(k)}$, because of the quadratic term in $\chi^{(k)}$ on the right-hand side of (8), since $u_1^{(k)}$ depends linearly on $\chi^{(k)}$. To tackle this we use the technique of H-measures to obtain the corrector term, see [5], involving the microstructure incorporated on the symmetric tensor M:

$$\int_\Omega C_0\varepsilon(u_2) : \varepsilon(\varphi)\,\mathrm{d}x = -\int_\Omega \theta C_0\varepsilon(u_1) : \varepsilon(\varphi)\,\mathrm{d}x + \int_\Omega \theta(1-\theta)C_0MC_0\varepsilon(u_0) : \varepsilon(\varphi)\,\mathrm{d}x \quad \forall\varphi\in V \tag{11}$$

with

$$M(x)\zeta : \zeta' = \int_{\mathsf{S}^{N-1}} m_0(\xi)\zeta : \zeta'\,\nu(x,\mathrm{d}\xi)$$

where we denote by S^{N-1} the unit sphere in $\mathbb{R}^N$ and for any $\zeta, \zeta' \in \mathcal{M}^{sym}_{N\times N}(\mathbb{R})$ we define

$$m_0(\xi)\zeta : \zeta' = \frac{\zeta\xi\cdot\zeta'\xi}{\mu_0} - \frac{(\lambda_0+\mu_0)(\zeta\xi\cdot\xi)(\zeta'\xi\cdot\xi)}{\mu_0(2\mu_0+\lambda_0)}$$

and ν being the H-measure associated to the sequence $\chi^{(k)} - \theta$, that converges weakly-$\star$ to zero. The microstructure is introduced in the relaxation of (10) through the measure ν and can be understood as a two point correlation. Thus, following [6], we introduce the adjoint state p_0 solution of

$$\int_\Omega C_0\varepsilon(p_0) : \varepsilon(\varphi)\,\mathrm{d}x = \int_\Gamma 2(u_0 - u^r)\cdot\varphi\,\mathrm{d}s \quad \forall\varphi\in V \tag{12}$$

This implies that

$$J^*_{sa}(\theta) = \int_\Gamma \|u_0 - u^r\|^2\,\mathrm{d}s - \eta\int_\Omega \theta C_0\varepsilon(u_0) : \varepsilon(p_0)\,\mathrm{d}x + \eta^2\int_\Gamma u_1\cdot u_1\,\mathrm{d}s - \eta^2\int_\Omega \theta C_0\varepsilon(u_1) : \varepsilon(p_0)\,\mathrm{d}x + \eta^2\int_\Omega \theta(1-\theta)\Phi\,\mathrm{d}x$$

where for each $x\in\Omega$, $\Phi(x)$ takes the minimum value of:

$$\Phi(x) = \min_{\xi\in\mathsf{S}^{N-1}} \big(m_0(\xi)C_0\varepsilon(u_0) : C_0\varepsilon(p_0)\big)(x)$$

We remark that the only participation of the microstructure is included in Φ and, moreover, that the values taken by this function are independent of θ, as u_0 and p_0 are likewise. This allows us to decouple the minimization on the microstructure, which is parameterized by ξ, and the spatial density distribution of the inclusion given by θ. Then we can compute the derivative of J^*_{sa} with respect to θ in order to obtain a gradient method. This is obtained by introducing a new adjoint state

$$\int_\Omega C_0\varepsilon(p_1) : \varepsilon(\varphi)\,\mathrm{d}x = \int_\Gamma 2u_1\cdot\varphi\,\mathrm{d}s \quad \forall\varphi\in V \tag{13}$$

Then the derivative in the direction $s\in L^\infty(\Omega)$ is given by

$$\frac{\partial J^*_{sa}}{\partial \theta}(s) = -\eta \int_\Omega sC_0\varepsilon(u_0) : \varepsilon(p_0)\,\mathrm{d}x - \eta^2 \int_\Omega s\big(C_0\varepsilon(u_0) : \varepsilon(p_1) + C_0\varepsilon(u_1) : \varepsilon(p_0)\big)\,\mathrm{d}x + \eta^2 \int_\Omega s(1-2\theta)\Phi\,\mathrm{d}x \tag{14}$$

With this last result, the construction of minimizing sequences for J^*_{sa} becomes possible through a gradient algorithm. The scheme of the algorithm is the following:

- Given $\theta^{(0)}$ and u^r on Γ, solve (6) and (12).
- Find the optimal lamination angle by calculating Φ.
- While $k \geqslant 1$ (until convergence), perform the following steps
  - (i) Solve for u_1 and p_1 to compute $\frac{\partial J^*_{sa}}{\partial \theta}(s)$ evaluated in $\theta = \theta^{(k-1)}$, in the direction s of a perturbation of θ.
  - (ii) Update the local proportion with a step size $\delta_k > 0$ by $\theta^{(k)} = \theta^{(k-1)} - \delta_k \frac{\partial J^*_{sa}}{\partial \theta} + \Lambda_k$, where the value of the Lagrange multiplier Λ_k is selected in order to enforce the volume constraint.
  - (iii) Evaluate $J^*_{sa}(\theta^{(k)})$: if it descends then go to (i), else, reduce the step size δ_k and go to (ii), until the step size be smaller than a given tolerance.
- Display the final results.

To compute $\partial J^*_{sa}/\partial\theta(s)$ in step (i), we must have previously selected the direction $s \in L^\infty(\Omega)$. Noticing that Eq. (14) is of the type

$$\frac{\partial J^*_{sa}}{\partial \theta}(s) = -\int_\Omega s\Pi\big(\eta, \theta, \varepsilon(u_0), \varepsilon(u_1), \varepsilon(p_0), \varepsilon(p_1)\big)\,\mathrm{d}x \tag{15}$$

we can simply set $s = \Pi$ a.e. in Ω to enforce the derivative to be always negative. This choice will ensure a descending direction for J^*_{sa}.

Unfortunately the performance of the method is strongly affected by the positions of both the load and of the sensors. For that reason we propose in the next section an adaptive strategy to select those locations.

3. An adaptive procedure

We now propose an adaptive procedure to select both, the positions of the displacement sensors and the place where load will be applied and its direction of application. This selection is made using the information available from previous measurements and their processing by the algorithm presented above. Therefore each major, or outer, iteration of the adaptive procedure consists of running the iterative algorithm of the previous section for a given location of the sensors and the load and for a given loading orientation. As it is explained below, the final result of this iterative algorithm will provide information to select either a new location of the sensors, or a new location and orientation of the load, to perform the following major iteration of the adaptive procedure.

Since numerical experience and physical intuition says that this method has a better performance when the real inclusion is close to where measurements are taken, we want to have a procedure to adjust such locations. However, the appropriate notion of "distance" is not obvious, because it might happen that the sample being tested has a complicated shape or topology. Then since the information being measured only travels inside the body, we think that it might be better to use the notion of geodesic distance, this is the distance between two points, but only travelling inside the body. Hence, if we call $d(x, \Gamma)$ the geodesic distance function, we define a quantity that measures the distance of the current guess for the inclusion to the measuring zone Γ as

$$H(\Gamma) = \int_\Omega \theta(x)\, d(x, \Gamma)\,\mathrm{d}x$$

Then $H(\Gamma)$ weights a proportion $\theta(x)$ at x by the geodesic distance of x to Γ. To compute $d(x, \Gamma)$ we use the fact that it is the positive and viscous solution of the eikonal equation

$$\big|\nabla d(x, \Gamma)\big| = 1 \quad \text{in } \Omega, \qquad d(x, \Gamma) = 0 \quad \text{on } \Gamma$$

We solve this problem numerically using the Fast-Sweeping method of Quian, Zhang and Zhao [10]. This method renders the computational cost of computing $d(x, \Gamma)$ negligible compared to solving the elasticity system in each iteration. The only major computational cost comes from the need to renumerate the nodes, but this is done only once for each detection problem. The minimum of H is obtained just by direct evaluation of $H(\Gamma)$ for different positions of Γ.

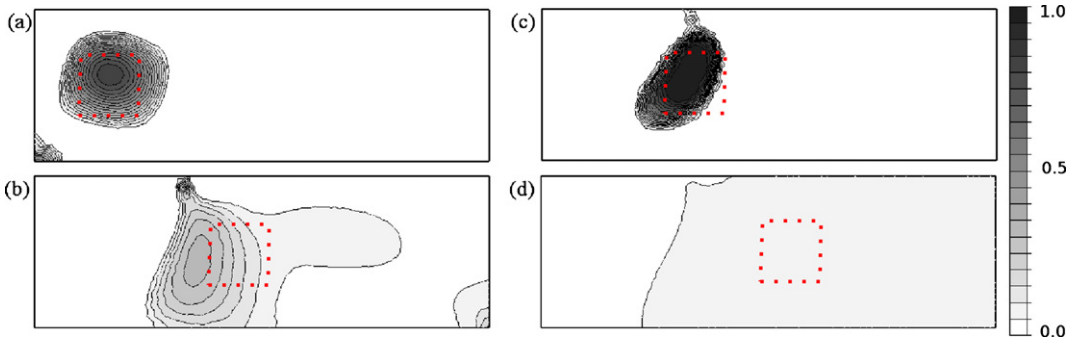

Fig. 1. Resulting inclusion density θ when detecting an inclusion located at different locations, marked with a dotted line, and subject to the same load.

On the other hand, we also have to select the location and direction of the load. This is done through an approximate maximization of the truncated expansion of the elastic energy (up to second order in η) on the current guess of the inclusion, by weighting at each point of Ω the elastic energy density by θ. Then, since

$$C^{eff} = C_0 + \eta\theta C_0 - \eta^2\theta(1-\theta)C_0MC_0 + o(\eta^2)$$

we get that

$$\begin{aligned}\mathcal{E}_{sa} &= \frac{1}{2}\int_\Omega \theta C^{eff}\varepsilon(u):\varepsilon(u)\,dx \\ &= \frac{1}{2}\int_\Omega \theta(1+\eta\theta)C_0\varepsilon(u_0):\varepsilon(u_0)\,dx + \eta\int_\Omega \theta(1+\eta\theta)C_0\varepsilon(u_0):\varepsilon(u_1)\,dx \\ &\quad - \frac{1}{2}\eta^2\int_\Omega \theta^2(1-\theta)C_0MC_0\varepsilon(u_0):\varepsilon(u_0)\,dx + \eta^2\int_\Omega \theta C_0\varepsilon(u_0):\varepsilon(u_2)\,dx + o(\eta^2)\end{aligned}$$

The loading zone will be selected by evaluating the truncation of $\mathcal{E}_{sa}$ for several positions of the load and choosing the one that gives the maximal value.

In order to obtain a quantitative comparison among different experimental settings, we introduce a positive number that gives us a simple measure of how much of the defect is placed by the method outside of its real location and how far from it it is placed:

$$\Psi(\theta) = \frac{\int_\Omega (1+\rho)(1-\chi^r)\theta\,dx + \int_\Omega (1-\theta)\chi^r\,dx}{\int_\Omega (1+\rho)(1-\chi^r)\,dx + \int_\Omega \chi^r\,dx}$$

Here ρ is the Euclidian distance function in $\mathbb{R}^N$ of a point in Ω from the set of the real location of the defect. Hence, the smaller Ψ is (being always nonnegative) means that we have a better performance of the method, taking value zero if and only if $\theta = \chi^r$. This function of the distribution θ uses the knowledge of the real location χ^r, then it is, of course, not used by the algorithm, but it provides a way to see the effectiveness of the adaptive method, better than the objective function for at least two reasons: first the objective function has been truncated and the relative importance of the neglected terms might be different from one major iteration to another and second, the experimental setting changes from each iteration and then the values taken by the truncated objective function are not truly comparable.

Before presenting the examples using adaptivity, we illustrate how sensitive is the optimization algorithm presented in the previous section to the position of the load. For that we did the following numerical experiment: Let a beam $\Omega = [0,3]\times[0,1]$, with dimensions in meters, be fixed on $\Gamma_D = \{(x,0):\ 0 \leqslant x \leqslant 3\}$ and let a uniform load be applied on the upper left third of the boundary, namely $\Gamma_N = \{(x,1):\ 0 \leqslant x \leqslant 1\}$. The inclusion is a square of side 0.4 m and the position of its successive centers are at the coordinates $(x, 0.5)$, with $x \in \{0.5, 1.0, 1.35, 1.65\}$ (Fig. 1(a)–(d)). To isolate the effect of the location of the load, we set $\Gamma = \partial\Omega \setminus \Gamma_D$, i.e., displacement is measured on all the accessible boundary. We use $E = 210$ GPa, $\nu = 0.3$ and $\eta = -0.1$, this is, the inclusion is 10% less stiff than the matrix.

We can see in Fig. 1 that the inclusion is fully detected in cases (a) and (b), while when it moves to the right it becomes more difficult to capture its successive locations. Recalling that the characteristic function associated with the exact location of the inclusion is χ^r and the exact displacement field is u^r, the energy stored inside and outside the inclusion are, respectively:

$$\mathcal{E}_{incl} = \frac{1}{2}\int_\Omega \chi^r C_1\varepsilon(u^r):\varepsilon(u^r)\,dx \quad \text{and} \quad \mathcal{E}_{out} = \frac{1}{2}\int_\Omega (1-\chi^r)C_0\varepsilon(u^r):\varepsilon(u^r)\,dx$$

Table 1
Evaluation of energies inside and outside the inclusion for different cases, following Fig. 1.

Case	Ψ	$\mathcal{E}_{incl}(\times 10^{-3})$	$\mathcal{E}_{out}(\times 10^{-3})$	$\mathcal{E}_{incl}/\mathcal{E}_{out} \times 100$
(a)	0.0219	7.65	42.83	17.85
(b)	0.0216	3.92	46.03	8.53
(c)	0.0682	0.99	48.63	2.03
(d)	0.0808	0.49	49.13	0.99

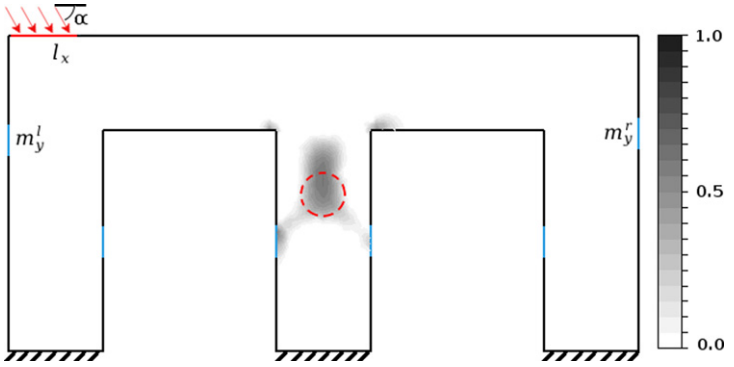

Fig. 2. Example 1: Inclusion density $\theta(x)$. Load is applied on the top of the structure (Γ_N, in red) and the localization of sensors (Γ, in blue).

The results displayed in Table 1 show a relationship between the energy and the ability of the method to capture the inclusion, where high energies in the inclusion can be related to good performance of the method.

4. Numerical examples

We present two applications where the matrix has $E = 210$ GPa and $\nu = 0.3$. We always start the algorithm with a plane distribution of the inclusion, namely θ is equal to a constant. Load is applied on part of Γ_N and with an angle α^o measured clockwise from the horizontal line, putting the zero angle to the right. The first example is about a frame with three columns and with the contrast parameter η taking value -0.1. The second example is about a perforated plate and with $\eta = -0.3$. The programming language we use is FreeFem++, see [11].

4.1. Example 1

We consider a frame 2 m wide and with a height 1 m. The width of each column and beam is 0.3 m. See Fig. 2, where we also show the distribution of θ after 4 iterations. The inclusion is a circle centered at $(1, 0.5)$ and radius 0.071 m, which represents 1.79% of the total area of the frame. Since $\eta = -0.1$, the Young modulus of the inclusion has a value equal to 0.9 times that of the matrix.

We use six displacement sensors, each of them measures over an interval of length 0.1 m and they are located on Γ_0, Γ_l and Γ_r. The position of the sensors on Γ_0 remain fixed, while the position of those in Γ_l and Γ_r are chosen among six possible positions. Then the measuring zone is $\Gamma = \Gamma_0 \cup \Gamma_l \cup \Gamma_r$, where

$$\Gamma_0 = \{0.3, 0.85, 1.15, 1.7\} \times [0.35, 0.45]$$
$$\Gamma_l = \left\{(0, y) \in \partial\Omega\colon\ m_y^l - 0.05 \leqslant y \leqslant m_y^l + 0.05\right\}$$
$$\Gamma_r = \left\{(2, y) \in \partial\Omega\colon\ m_y^r - 0.05 \leqslant y \leqslant m_y^r + 0.05\right\}$$

Load is applied on an interval of length 0.2 m and we select among six uniformly spaced possible positions for Γ_N and among five different angles to orient the load. Then we have that Γ_N is parameterized as $\Gamma_N = \{(x, 1) \in \partial\Omega\colon\ l_x - 0.1 \leqslant x \leqslant l_x + 0.1\}$.

The successive positions of the load and measure zones are presented in Table 2.

In this case, the most important improvement is obtained in the first iteration, however, the successive changes in boundary conditions improve this result, diminishing the final value of Ψ. The location of the inclusion is very well recovered and adaptivity is indeed helpful. In Fig. 3 each curve is associated to an outer or major iteration and it can be interpreted as the continuation of the previous curve. The horizontal axis represents the iterations of the algorithm of Section 2, this is, for a given position of sensors and loads and a given orientation of the load.

Table 2
Example 1: Center of the zones of the adjustable sensors, Γ_l parameterized by m_y^l and Γ_r parameterized by m_y^r. Center of the loading zone Γ_N parameterized by l_x.

Iteration	m_y^l	m_y^r	l_x	α	Ψ
0	0.35	0.35	1.5	45	0.01497
1	0.35	0.35	1.61	170	0.00899
2	0.69	0.69	1.61	170	0.00898
3	0.69	0.69	0.12	10	0.00901

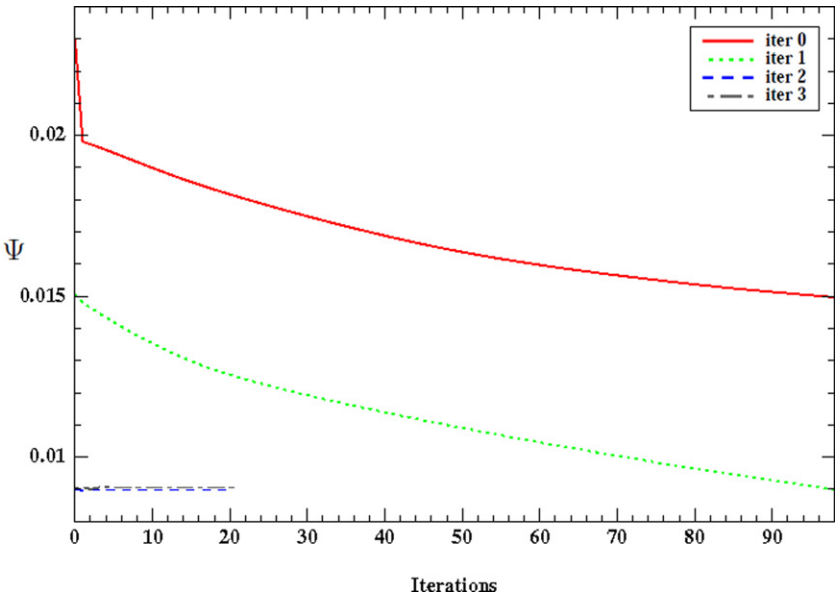

Fig. 3. Example 1: Evolution of Ψ.

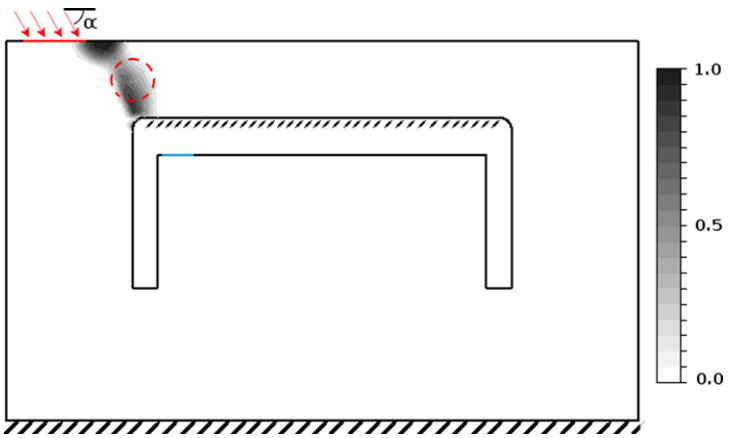

Fig. 4. Example 2: Inclusion density $\theta(x)$.

4.2. Example 2

Now we consider a rectangular plate of width equal to 2 m and height of 1.2 m, but with a perforation shaped as an inverted U. The area of the perforated plate is 2.19 m^2. The upper boundary of the perforation is fixed and displacements are only measured on the lower horizontal boundary of the perforation with $y = 0.84$. See Fig. 4.

The loading zone has length 0.2 m and its center is denoted by l. The measuring zone has length 0.1 m and its center is denoted by m. The successive positions of the load and measure zones are presented in Table 3. The inclusion is a circle centered at $(0.4, 1.08)$ and radius 0.071 m, which represents 0.72% of the total area of the perforated plate. Since $\eta = -0.3$, the Young modulus of the inclusion has a value equal to 0.7 times that of the matrix.

Table 3
Example 2: Center of Γ represented by m. Center of Γ_N represented by l.

Iteration	m	l	α	$\Psi(\times 10^{-3})$
0	1	0.6	90	6.33
1	1	0.154	10	4.59
2	0.644	0.154	10	4.27
3	0.644	0.154	170	4.76
4	0.543	0.154	170	4.96
5	0.543	0.154	10	4.32
6	0.644	0.154	10	4.28
7	0.644	0.154	170	4.66
8	0.543	0.154	170	4.75
9	0.543	0.154	10	4.31

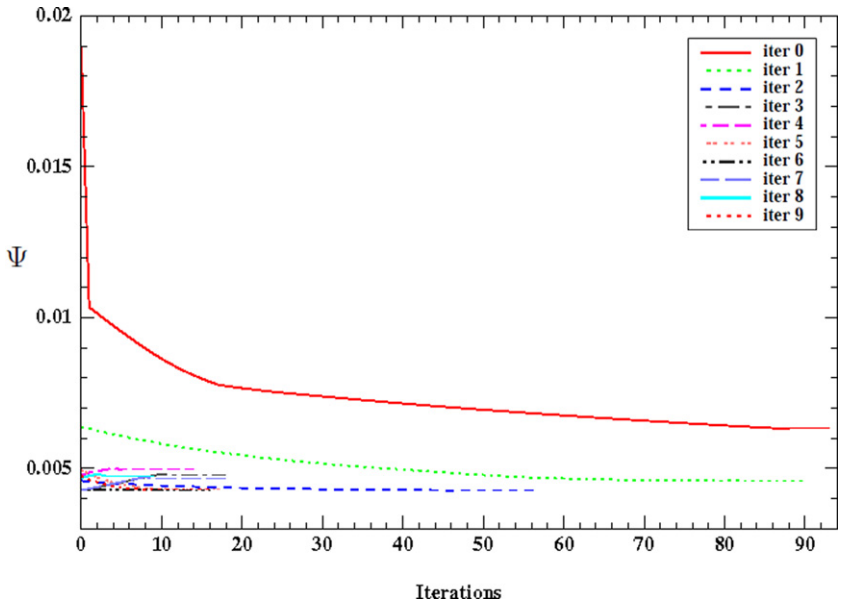

Fig. 5. Example 2: Evolution of Ψ.

From the values attained by Ψ displayed on Table 3 and depicted in Fig. 5, we see that no improvement on the quality of the guess is gained after the third iteration. For the recovery of this defect the method did very well, and adaptivity is again very useful. However if the defect is further away from the loading zone, it becomes very difficult to find it. The reason being that this problem is quite hard, since the displacement field "has to turn" to reach the sensor on the other side of the perforation.

5. Concluding remarks

The proposed adaptive method is indeed capable of detecting the presence of small inclusions having a relatively small contrast in stiffness with respect to the surrounding matrix. However the inclusion needs to be close to places where load can be applied. There is some dependency on the initial guess for the distribution at the beginning of the optimization process, then, in absence of more information, it is better to start the method from a plane distribution of the defect. The running time for triangular meshes having 5000 triangles is of the order of 20 minutes on a standard PC.

There are two sensitive aspects on the implementation of the algorithm. First, we do not impose that the optimization algorithm be of strict descent, to allow it to exit from local minima, however if one allows for large increments on the value of the objective function, sometimes the method becomes unstable. The second issue, that is connected to the previous, is about the stopping criteria. It is very hard to set a general criteria.

Using the geodesic distance to select the positions of the sensors represents a small additional computational cost and it is not clear that we gained much by using it, since we run the two examples shown using instead the Euclidian distance and no big difference was observed. However this point needs further analysis.

The stability of the algorithm from Section 2 under noise measurement and ill characterization of the defect, namely an erroneous volume or contrast, are studied in [7] and the algorithm is quite robust if η is not too small, this is, for $\eta = \pm 0.1$ the algorithm performs well, while for $\eta = \pm 0.01$ the algorithm becomes unstable.

One could do several loading experiments and then process the information as a multi-load problem, this is, to select θ to minimize the sum of the misfits for each experiment, and then decide whether to adapt the positions of the sensors and loads.

Acknowledgements

Both authors thank an anonymous referee for interesting comments. S.G. thanks the financial support of the Fondecyt research grant number 1090334, of the Chilean state. J.M. thanks the Conicyt fellowship for support during his doctoral studies.

References

[1] M. Burger, S. Osher, A survey on level set methods for inverse problems and optimal design, European J. Appl. Math. 16 (2) (2005) 263–301.
[2] R. Gallego, G. Rus, Identification of cracks and cavities using the topological sensitivity boundary integral equation, Comput. Mech. 33 (2) (2004) 154–163.
[3] B. Guzina, M. Bonnet, Topological derivative for the inverse scattering of elastic waves, Quart. J. Mech. Appl. Math. 57 (2) (2004) 161–179.
[4] S. Gutiérrez, J. Mura, Small amplitude homogenization applied to inverse problems, Comput. Mech. 41 (5) (2008) 699–706.
[5] L. Tartar, H-measures, a new approach for studying homogenisation, oscillations and concentration effects in partial differential equations, Proc. Roy. Soc. Edinburgh Sect. A 115 (1990) 193–230.
[6] G. Allaire, S. Gutiérrez, Optimal design in small amplitude homogenization, M2AN Math. Model. Numer. Anal. 41 (3) (2007) 543–574.
[7] J. Mura, S. Gutiérrez, Detection of weak defects in elastic bodies through small amplitude homogenization, submitted for publication.
[8] G. Allaire, Shape Optimization by the Homogenization Method, Springer-Verlag, 2002.
[9] L. Tartar, Remarks on optimal design problems, in: Calculus of Variations, Homogenization and Continuum Mechanics, Marseille, 1993, in: Ser. Adv. Math. Appl. Sci., vol. 18, World Sci. Publishing, River Edge, NJ, 1994, pp. 279–296.
[10] J. Qian, Y.-T. Zhang, H.-K. Zhao, Fast sweeping methods for eikonal equations on triangular meshes, SIAM J. Numer. Anal. 45 (1) (2007) 83–107.
[11] F. Hecht, O. Pironneau, A. Le Hyaric, K. Ohtsuka, FreeFem++, code and user manual freely available at http://www.freefem.org.